Available online at www.sciencedirect.com

SciVerse ScienceDirect

Procedia Engineering 27 (2012) 1169 – 1178

Procedia Engineering

www.elsevier.com/locate/procedia

2011 Chinese Materials Conference

Microstructural control and properties optimization of high-entrop alloys

Yong Zhang[a,*] Wei jie Peng[b]

[a,b]*State Key Laboratory for Advanced Metals and Materials, University of Science and Technology Beijing, 100083, China*

Abstract

A criterion for the solid-solution phase formation in the high-entropy alloys was proposed based on two parameters Ω>1.1 and δ<6.6%. Here, $\Omega = \frac{T_m \Delta S_{mix}}{|\Delta H_{mix}|}$, and $\delta = \sqrt{\sum_{i=1}^{n} c_i (1 - r_i / \bar{r})^2}$ .The high-entropy alloys of TiZrNb, CoCrFeNiCu, and $CoFeNi(AlSi)_x$ (X=0.2, 0.5) were prepared by arc-melting and copper mold casting. It was found that the tensile yield strength of the TiZrNb alloy was 872MPa, and tensile modulus was 45GPa. The properties of CoCrFeNiCu alloys can be optimized by multiple processing, such as cold rolling, annealing, and water quenching. Based on the HE(high-entropy) conception, a soft magnetic alloy $CoFeNiAl_xSi_x$ was developed.

Keywords: High-entropy alloys; substitutional alloys; solid-solution; Tensile properties; Magnetic properties

1. Introduction

In recent years, high-entropy alloys (HE alloys) have attracted increasing attentions because of their unique properties [1-16], such as high temperature strength[6, 14], high corrosion and wear resistances, superparamagnetic properties [2], etc. These properties make the HE alloys potentially used as the coatings at the high temperature, and shielding materials for low excursion four-mode ring laser gyro[17]. The HE alloys usually contain five or more elements; and keep the alloys with HE of mixing at the liquid state. HE alloys usually form solid-solution as their main phase rather than the intermetallic compounds. This

* Corresponding author. Tel.: +86-10-62334927; fax: +86-10-62332508.
E-mail address: drzhangy@ustb.edu.cn.

 doi:10.1016/j.proeng.2011.12.568

random solid-solution phase is of chemical disorder, while the amorphous phase is of topological disorder. Anyway, the order parameters, such as long-range-order parameter, and short-range-order parameter, are very important to indicate the phase structures.

The definition for the HE alloys has been extended to a more open conception in recent years, e.g. the four or fewer principle elements alloys, in another word, medium-entropy alloys, e.g. NbWMoTa [4, 6], and one of the elements content can be in a range from 5 % to 60 %, e.g. $Fe_6CoCrNiAlTiSi$ [18], $Al_3CoCrFeNi$ [19]. Some typical HE alloys were listed in Table 1.

Table 1. Some typical HE alloys compositions, phases, and mechanical properties, processing

Compositions	Phases	Yield Strength or Hardness	Samples and preparations	reference
AlCoCrFeNi	BCC	1500 MPa	Copper mold casting	1
CoCrFeNiCu	FCC	230 MPa	Copper mold casting	2
AlCoCrFeNiCu	BCC+FCC	950 MPa	Arc-melting	3
NbMoTaW	BCC	1058 MPa, HV4460	Arc-melting	4, 6
VNbMoTaW	BCC	1246MPa, HV5520	Arc-melting	4, 6
$Fe_6NiCoSiAlTi$	BCC	HV800	Coating by laser cladding	18
$Al_3CoCrFeNi$	BCC	HV506	Arc-melting	19
$CoCrFeNiCu_{0.5}$	FCC	HV174	Arc-melting	20
$Al_{0.5}CoCrFeNi$	FCC	HV247	Arc-melting	21

As the main characteristics for the HE alloys is the HE of mixing at the liquid state, and the content of the alloying elements is very high. The conception of HE alloys provides a new point of view to study and develop the alloys with special properties. In the paper, TiZrNb and $CoFeNiAl_xSi_x$ alloys were designed. We provide examples to show that the properties of the HE alloy can be largely adjusted by multiple processings, e.g. cold rolling and annealing.

2. Experimental

Ingots with nominal composition of TiZr, TiZrNb, TiZrNbMo, TiZrNbMoV, $TiZrNbMoV_{0.5}$, TiZrNbMoVAl, CoCrFeNiCu, and $CoFeNi(AlSi)_x$ (x values in molar ratio, x=0.2, 0.5, all the alloys are in molar ratio) were prepared by arc melting pure elements with a purity higher than 99.5wt% under high-purity argon atmosphere on a water-cooled Cu hearth. The alloys were re-melted several times in order to obtain homogeneity. Cylindrical rods with a diameter of 5 mm were prepared by the copper-mould suction casting. Microstructure investigations of the cylindrical alloys were carried out by X-ray diffraction (XRD) using a PHILIPS APD-10 diffractometer with Cu-Kα radiation. Cylindrical samples of $\phi 5 \times 10$ mm^2 were prepared for compressive tests and investigated using MTS 809 materials testing machine at room temperature with a strain rate of 2×10^{-4} s^{-1}. The morphologies of cross sections and fracture surfaces were examined using a LEO-1540 scanning electron microscope (SEM) with energy dispersive spectrometry (EDS). The magnetization curves were measured by LDJ 9600 vibrating sample magnetometer.

3. Results

3.1. Phase formation criterion

Previous work has reported the phase formation zones for the HE alloys [11], the small atomic size differences (δ) and near-zero values of the absolute enthalpy of mixing (ΔHmix) facilitate the formation of solid-solutions for HE alloys. Recently, a parameter Ω [12, 13] was proposed which combined the effects of entropy of mixing and the enthalpy of mixing for predicting the solid-solution phase formation among various multi-component alloys,

$$\Omega = \frac{T_m \Delta S_{mix}}{\left|\Delta H_{mix}\right|} \tag{1}$$

$$T_m = \sum_{i=1}^{n} c_i (T_m)_i \tag{2}$$

Here, $(T_m)_i$ and c_i are the melting point and molar percent of the ith component, respectively.

The atomic size difference δ in n-element alloy is express as follows:

$$\delta = \sqrt{\sum_{i=1}^{n} c_i (1 - r_i / \bar{r})^2} \tag{3}$$

$$\bar{r} = \sum_{i=1}^{n} c_i r_i \tag{4}$$

Where r_i is the atomic radius of the ith component. Figure 1 presents a map summarized by 174 multi-component alloys in a Ω and δ coordinate system. According to Fig 1, the random solid-solution phase forms in a zone of Ω ≥ 1.1 and δ ≤ 6.6 %. For the formation of intermetallics and bulk metallic glasses, the δ is in the range of about 7% to 14%. However, the Ω values for the intermetallics higher than that of the bulk metallic glasses.

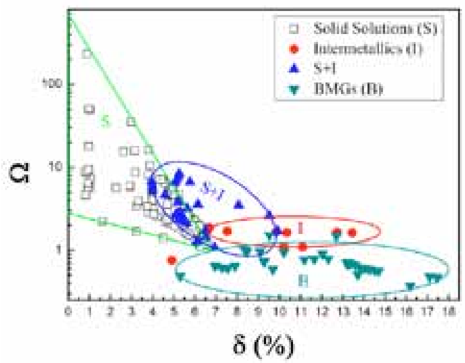

Figure. 1. A phase formation map of solid-solution (S), intermetallics (I), and bulk metallic glasses (B) in a Ω-δ coordination system for multi-component alloys [23]

3.2. TiZrNb based HE alloys

Figure 2 (a) shows the XRD patterns for the TiZr based equiatomic ratio alloys with increased number of components. We can see that all the samples mainly contain BCC phases. This is due to the HE and the low enthalpy of mixing effects of the alloy systems. As the mentioned above the random solid-solution phase forms in a zone of $\Omega \geq 1.1$ and $\delta \leq 6.6$ %. The Ω and δ values of the alloys were listed in Table 2.

From Table 2, we can see that the value of Ω for the TiZr binary alloy is very large, this is due to the enthalpy of mixing (ΔH_{mix}) between Ti and Zr is 0. Moreover, we can see that all the TiZr based alloys located in the zone for the forming of random solid-solution, that is: $\Omega \geq 1.1$ and $\delta \leq 6.6$ %. The Ω values for the Al containing alloys are relatively low compared to the Al free alloys. The reasons may be as following: 1, The enthalpy of mixing of Al with other elements are more negative, and the absolute value is very large; 2,The low melting point of Al lead to the low value of T_m. It should be noticed that some other phase diffraction peaks can be observed besides the BCC peaks. This indicates that the low value of Ω may correspond to the reduced HE effect of the alloy, and this may not be benefit to the HE stablized solid-solution phase.

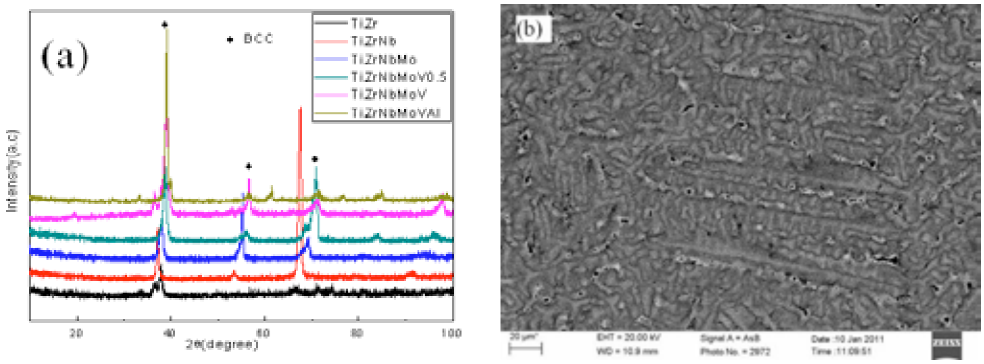

Figure. 2. XRD patterns for the TiZr, NbTiZr, NbTiZrMo, TiZrNbMoV0.5, TiZrNbMoV, and TiZrNbMoVAl alloys(a), and SEM picture for the TiZrNbMoV alloy(b)

Figure 2 (b) shows the SEM image for the TiZrNbMoV alloy, showing the typical dendrite morphology. Figure 3 (a) shows the compressive stress-strain curve of TiZrNb equi-atomic ratio alloy. We can see that the alloy exhibits a yield strength of about $\sigma_{0.2}$=690 MPa, and a compressive Young's modulus of E_C=75 GPa. The ductility of the alloy is so good that no fracture occurs during the compression. Figure 3 (b) shows the tensile stress-strain curve for the TiZrNb equi-atomic ratio alloy. We can see that the alloy exhibits the tensile yield strength of $\sigma_{0.2}$=872 MPa, tensile elongation δ=7%, tensile fracture strength σ_b=970 MPa, and the tensile Young's modulus E_T=45 GPa. Figure 3 (c) shows the typical fracture surface of the tensile samples, which is of the dimple morphology. The significant elastic asymmetry in tension and compression for the TiZrNb based alloy was also reported in Ref.[23].

Table 2. Parameters such as enthalpies of mixing (ΔHmix), entropies of mixing (ΔSmix), Ω, atomic radius difference (δ) , incorporate phases for the alloy series.

Alloys	ΔHmix(KJ/mol)	ΔSmix(J/K.mol)	Ω	δ（%）	Phase(s)
TiZr	0	5.76	∞	3.63	BCC
TiZrNb	2.67	9.13	7.79	4.05	BCC
TiZrNbMo	-2.50	11.52	11.21	5.20	BCC
TiZrNbMoV0.5	-2.67	13.14	11.83	5.59	BCC
TiZrNbMoV	-2.72	13.38	11.71	5.71	BCC
TiZrNbMoVAl	-14.44	14.89	2.22	5.22	BCC
CoCrFeNiAl	-12.32	13.38	1.52	5.32	BCC
CoCrFeNiAlNb0.1	-13.32	13.88	1.48	5.62	BCC
CoCrFeNiAlNb0.5	-16.58	14.71	1.33	6.46	BCC+Laves

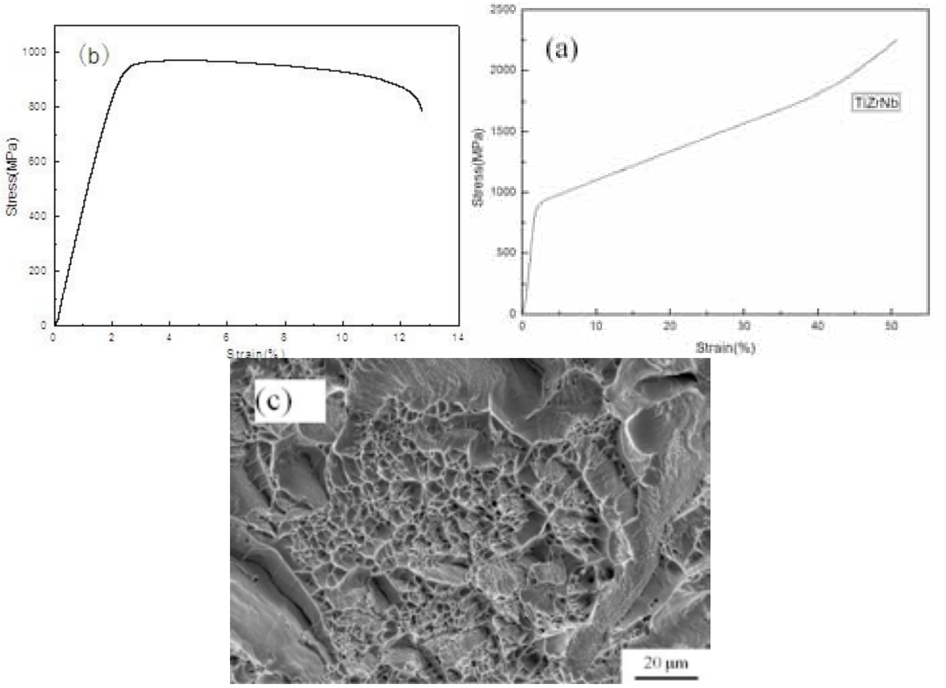

Figure. 3. Compressive (a), tensile (b) stress-strain curves, and the fracture surface of the tensile sample (c) for the TiZrNb equi-atomic ratio alloy. The size of the compression sample is ϕ5×10 mm, and the tensile sample is with thickness of the sample of 2 mm, the width of 4 mm, and the gage length is about 12 mm.

3.3. Cold Rolling and Heat treatments

The tensile properties of the CoCrFeNiCu HE alloy samples with five states were studied, and the condition of the samples were A: as prepared by arc-melt state; B: 700 °C annealed 5 hours and furnace cooled; C: 700 °C annealed 5 hours and water quenching; D: cold rolling with deformation of 50%; E: cold rolling with deformation of 50%, and then 300°C annealed 5 hours and furnace cooled, respectively.

Figure 4 (a) shows the typical tensile sample for the tensile tests. The thickness of the sample is 2 mm, the width is 4 mm, and the gage length is 12 mm. Figure 4 (b) shows the tensile stress-strain curves for the five states of the alloys. It can be seen that as arc-melt sample exhibits the lowest tensile yield strength ($\sigma_{0.2}$=350 MPa) and tensile elongation (δ=13%). After annealing, the tensile elongation increased apparently to be about δ=35%. The tensile yield strength slightly increased to be about $\sigma_{0.2}$=450 MPa with processing of C. It should be noticed that the main difference between the processing of B and C is the cooling rates. The high cooling rate may lead to the finer size of the precipitations, and enhancing the dispersion strengthening effect. Figure 4 (b) shows that the alloy exhibits the highest tensile yield strength for cold rolling state, which is about $\sigma_{0.2}$=900 MPa, however, the tensile elongation was significantly decreased to be about δ=7%. The tensile yield strength was slightly decreased and the tensile elongation was slightly increased after 300°C annealed 5 hours and furnace cooling. Figure 5 shows the fracture surface of the tensile samples, It has been found that the dimples and dendrite arms which were induced by the tensile loading, indicating the tensile ductility of the alloys.

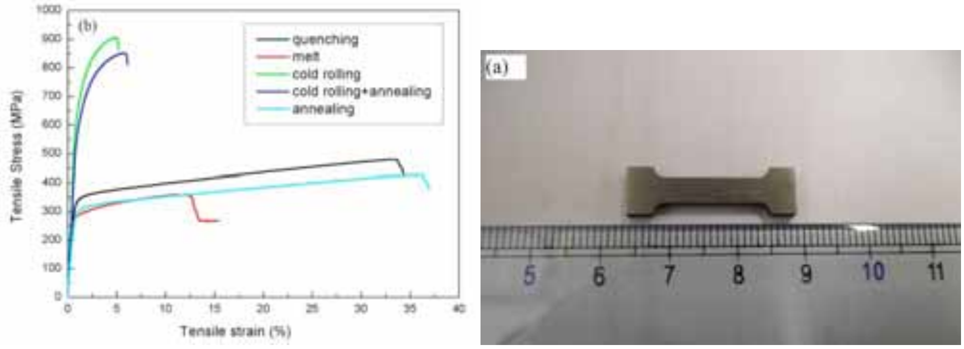

Figure. 4. The tensile sample (a) and tensile stress-strain curves (b) for the CoCrFeNiCu HE alloy. The thickness of the sample is 2 mm, the width is 4 mm, and the gage length is about 12 mm.

3.4. CoFeNiAlSi magnetic alloys

Figure 6 shows the XRD patterns of the $CoFeNiAl_{0.2}Si_{0.2}$ and $CoFeNiAl_{0.5}Si_{0.5}$ alloys. For the $CoFeNiAl_{0.2}Si_{0.2}$ alloy (a, b), the FCC reflection peaks are very apparent, there is a small peak near the first peak of the pattern (b), as patterns (a) and (b) are the same alloy, but two ingots. It has been found that the alloys were very sensitive to the dynamic factors, e.g. cooling rates. For the $CoFeNiAl_{0.5}Si_{0.5}$ alloy, the FCC reflections were shifted to the high angle side, this may be attributed to that more Al and Si additions will make the lattice shrink. For all the two alloys, we can not see the super lattice peaks, which indicates the long-range ordering of the alloys. Figure 7 shows the metallurgraphic pictures of the two alloys. For the $CoFeNiAl_{0.2}Si_{0.2}$ alloys, the microstructure is typical dendrite which was uniformly distributed and with arm size of about 50 μm; while for the alloy of $CoFeNiAl_{0.5}Si_{0.5}$, it shows the typical grains, with grain size of about 200 μm, and in the grains, there are typically two or three dendrites in each grain. Figure 8 shows the compressive stress-strain curves for the two alloys, we can see that the $CoFeNiAl_{0.2}Si_{0.2}$ alloy is ductile and has a very large work hardening capacity, while the alloy of $CoFeNiAl_{0.5}Si_{0.5}$, is very brittle, and after the compressive tests, the samples were crushed to be powders. Figure 9 shows the magnetic hysteresis loops of the two alloys. For the $CoFeNiAl_{0.2}Si_{0.2}$ alloy, the saturation magnetization Ms=1.151 T，the coercivity Hc=1400.72 A/m，and remanence magnetization Mr=0.01163 T; while for the $CoFeNiAl_{0.5}Si_{0.5}$ alloy, the saturation magnetization Ms= 0.731 T，the coercivity Hc=1937 A/m，and remanence magnetization Mr=0.01307 T. These properties show the alloys are typical soft magnetic alloys [24].

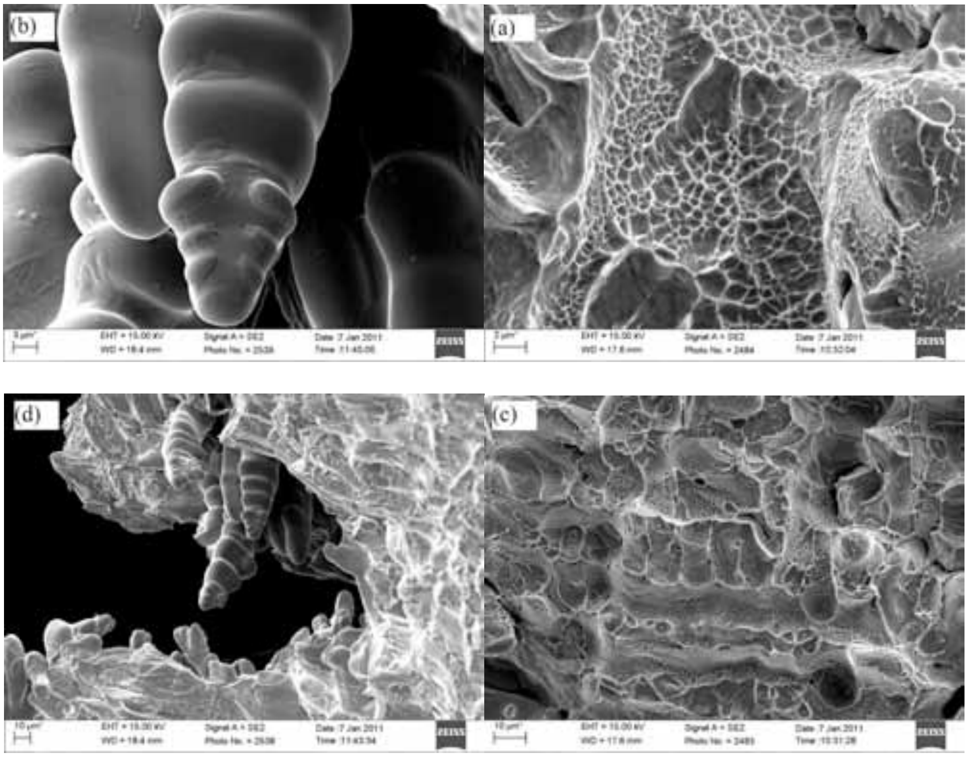

Figure. 5. The fracture morphologies for the CoCrFeNiCu HE alloy under the tension loading.

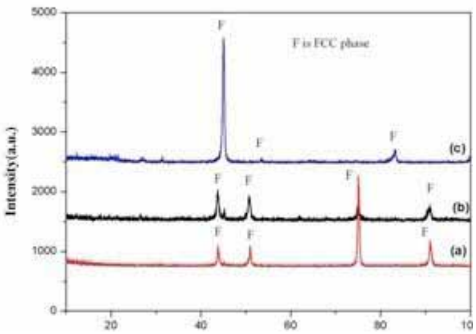

Figure. 6. XRD Patterns of the $CoFeNiAl_{0.2}Si_{0.2}$ (a, b) and $CoFeNiAl_{0.5}Si_{0.5}$ alloys

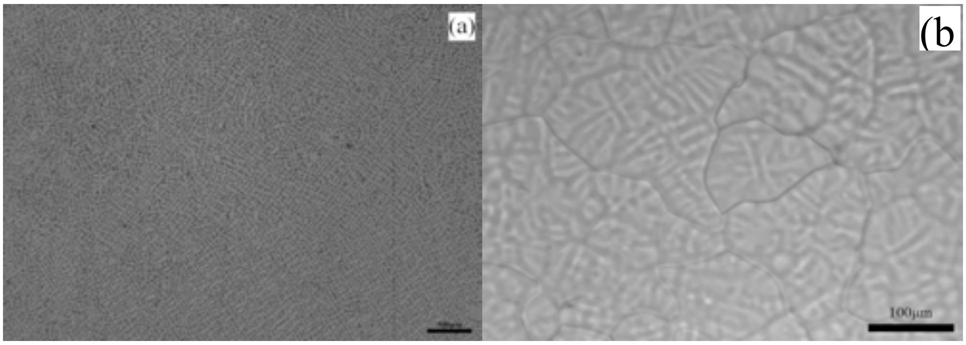

Figure. 7. Metallurgraphic pictures of the $CoFeNiAl_{0.2}Si_{0.2}$ (a) and $CoFeNiAl_{0.5}Si_{0.5}$ (b) alloys

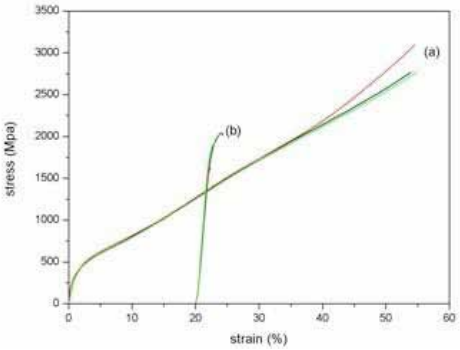

Figure. 8. Compressive stress-strain curves of the $CoFeNiAl_{0.2}Si_{0.2}$ (a) and $CoFeNiAl_{0.5}Si_{0.5}$ (b) alloys, the sample size is ϕ5×10 mm.

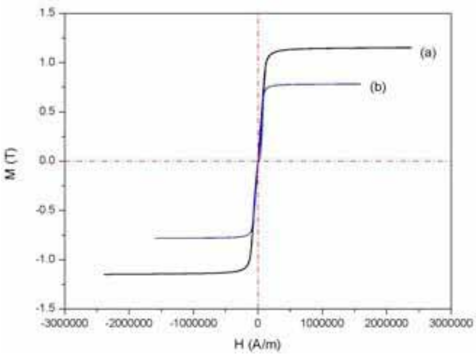

Figure. 9. Magnetization curves of the CoFeNi $Al_{0.2}Si_{0.2}$ (a) and $CoFeNiAl_{0.5}Si_{0.5}$ (b) alloys

4. Discussions

The phase predicting before the experiments is very important for the design of HE alloys [25, 26]. However, many criteria are based on some parameters which can only be obtained after the alloy was prepared. The random solid-solution phase forms in a zone of $\Omega \geq 1.1$ and $\delta \leq 6.6$ %, and the parameters, Ω and δ can be calculated by using the parameters for the constitute elements. Fortunately, the parameters, such as the radius of the elements, the entropy of mixing, the enthalpy of mixing, are available before doing the experiments, therefore this criteria will be helpful to developing of the advanced metallic alloys.

In order to optimizing the properties of the alloys, the composition of the alloys should be first optimized. Based on the HE effect, the number of the constitute elements was changed in the present investigation. It was obvious that when the values of Ω and δ kept in the zone for the formation of solid-solution, almost all the alloys including the alloys of TiZr, TiZrNb, TiZrNbMo, $TiZrNbMoV_{0.5}$, TiZrNbMoV, and TiZrNbMoVAl are BCC solid-solution as the main phase, especially that the ternary TiZrNb equi-atomic ratio alloy exhibits excellent tensile strength and elongation.

Process controlling is usually used to optimize the microstructure and properties of the materials, e.g. water quenching can eigher get the steels hardening, or get the Cu alloys softening. The alloys prepared by casting are usually used as the thin casings rather than the important structural parts. The deformed state of the alloys, e.g. by rolling and forging, usually have uniform microstructures, and exhibit better mechanical properties and engineering reliability. From Fig. 8, it can be observed that the tensile yield strength of the HE alloy can be effectively improved by the cold rolling.

Based on the conception of HE and equi-atomic ratio, the soft magnetic alloys may need revisited. The results shows that the lattice paramters can be easily adjusted by changing the contents of the Al and Si, and a rather soft magnetic HE alloy was obtained, which is $CoFeNiAl_{0.2}Si_{0.2}$, this may suggest a new way for developments of the high performance magnetic alloys.

5. Conclusions

TiZrNb equi-atomic ratio alloy exhibits the tensile yield strength of 872 MPa, and tensile elongation of 7%. The tensile fracture strength is about 970 MPa, and the tensile Young's modulus is about 45 GPa. The mechanical properties of HE alloy of CoCrFeNiCu can be tailured by cold rolling, annealing, and water quenching. $CoFeNiAl_{0.2}Si_{0.2}$ HE alloy with high ductility, large work hardening capacity, and good soft magnetic properties were developed. The solid-solution phases formation criteria for the multi-component alloys: $\Omega \geq 1.1$ and $\delta \leq 6.6$ %, is applicable for the development of new alloys.

References

[1] Zhou YJ, Zhang Y, Wang YL, Chen GL. Solid solution alloys of $AlCoCrFeNiTi_x$ with excellent room-temperature mechanical properties. *Applied Physics Letters* 2007;**90(18)**:181904-3.

[2] Wang XF, Zhang Y, Qiao Y, Chen GL. Novel microstructure and properties of multicomponent $CoCrCuFeNiTi_x$ alloys. *Intermetallics* 2007;**15(3)**:357-362.

[3] Yeh JW, Chen SK, Lin SJ, Gan JY, Chin TS, Shun TT, Tsau CH, Chang SY. Nanostructured high-entropy alloys with multiple principal elements: Novel alloy design concepts and outcomes. *Advanced Engineering Materials* 2004;**6(5)**:299-303.

[4] Senkov ON, Wilks GB, Scott JM, Miracle DB. Mechanical properties of $Nb_{25}Mo_{25}Ta_{25}W_{25}$ and $V_{20}Nb_{20}Mo_{20}Ta_{20}W_{20}$ refractory high entropy alloys. *Intermetallics* 2011;**19**:698-706.

[5] Singh S, Wanderka N, Murty BS, Glatzel U, Banhart J. Decomposition in multi-component AlCoCrCuFeNi high-entropy alloy. *Acta Materialia* 2011;**59**:182–190.

[6] Senkov ON, Wilks GB, Miracle DB, Chuang CP, Liaw PK. Refractory high-entropy alloys. *Intermetallics* 2010;**18(9)**:1758-1765.

[7] Cantor B, Chang ITH, Knight P, Vincent AJB. Microstructural development in equiatomic multicomponent alloys. *Materials Science and Engineering A* 2004;**375-377**:213-218.

[8] Yeh JW, Lin SJ, Chin TS, Gan JY, Chen SK, Shun TT, Tsau CH, Chou SY. Formation of simple crystal structures in Cu-Co-Ni-Cr-Al-Fe-Ti-V alloys with multiprincipal metallic elements. *Metallurgical and Materials Transactions A* 2004;**35(8)**:2533-2536.

[9] Li C, Li JC, Zhao M, Jiang Q. Effect of alloying elements on microstructure and properties of multiprincipal elements high-entropy alloys. *Journal of Alloys and Compounds* 2009;**475(1-2)**:752-757.

[10] Chang HW, Huang PK, Davison A, Yeh JW, Tsau CH, Yang CC. Nitride films deposited from an equimolar Al-Cr-Mo-Si-Ti

alloy target by reactive direct current magnetron sputtering. *Thin Solid Films* 2008;**516(18)**:6402-6408.
[11] Zhang Y, Zhou YJ, Lin JP, Chen GL, Liaw PK. Solid-solution phase formation rules for multi-component alloys. *Advanced Engineering Materials* 2008;**10(6)**:534-538.
[12] Zhang Y, Chen GL, Gan CL. Phase Change and Mechanical Behaviors of $Ti_xCoCrFeNiCu_{1-y}Al_y$ High Entropy Alloys. *Journal of ASTM International* 2010;**7(5)**, JAI102527.
[13] Zhang Y. Mechanical Properties and Structures of High Entropy Alloys and Bulk Metallic Glasses Composites. *Materials Science Forum* 2010;**654-656**:1058-1061.
[14] Zhang Y, Zhou YJ. Solid Solution Formation Criteria for High Entropy Alloys. *Materials Science Forum* 2007;**561-565**:1731-1739.
[15] Zhang Y, Zhou YJ, Hui XD, Wang ML, Chen GL. Minor alloying behavior in bulk metallic glasses and high-entropy alloys. *Science in China, Series G* 2008;**51(4)**:427-437.
[16] Cai H, Zhang H, Zheng Y. Soft magnetic devices applied for low excursion four-mode ring laser gyro. *IEEE Transaction on Magnetics* 2007;**43(6)**:2686-2688.
[17] Zhang H, Pan Y, He Y, Jiao H. Microstructure and properties of 6FeNiCoSiCrAlTi high-entropy alloy coating. *Applied Surface Science* 2011;**257:**2259-2263.
[18] Li C, Li JC, Zhao M, Jiang Q. Effect of alloying elements on microstructure and properties of multiprincipal elements high-entropy alloys. *Journal of Alloys and Compounds* 2009;**475**:752-757.
[19] Lin C, Tsai H, Bor H. Effect of aging treatment on microstructure and properties of high-entropy $Cu_{0.5}CoCrFeNi$ alloy. *Intermetallics* 2010;**18**:1244-1250.
[20] Lin C, Tsai H. Evolution of microstructure, hardness, and corrosion properties of high-entropy $Al_{0.5}CoCrFeNi$ alloy. *Intermetallics* 2011;**19**:288-294.
[21] Zhang YW, Li SJ, Obbard EG, Wang H, Wang SC, Hao YL, Yang R. Elastic properties of Ti–24Nb–4Zr–8Sn single crystals with bcc crystal structure. *Acta Materialia* 2011;**59**:3081–3090.
[22] Aykol M, AkdenizMV, Mekhrabov AO. Solidification behavior, glass forming ability and thermal characteristics of soft magnetic FeCoBSiNbCu bulk amorphous alloys. *Intermetallics* 2011;**19**:1330-1337.
[23] Peng WJ, Zhang Y. Micro-alloying of yttrium in Zr-based bulk metallic glasses. *Progress in Natural Science-Materials International* 2011;**20(1)**:46-52.
[24] Zhang Y, Xu W, Tan H, Li Y. Microstructure control and ductility improvement of La-Al-(Cu,Ni) composites by Bridgman solidification. *Acta Materialia* 2005;**53**:2607-2616.